INSTITUTE OF PHYSICS PUBLISHING SEMICONDUCTOR SCIENCE AND TECHNOLOGY

Semicond. Sci. Technol. **21** (2006) 429–436 doi:10.1088/0268-1242/21/4/004

A kinetic approach to tunnelling at Schottky contacts

A Domaingo and F Schürrer

Institute of Theoretical and Computational Physics, Graz University of Technology, Petersgasse 16, 8010 Graz, Austria

E-mail: domaingo@itp.tu-graz.ac.at and schuerrer@itp.tu-graz.ac.at

Received 23 December 2005, in final form 3 January 2006
Published 21 February 2006
Online at stacks.iop.org/SST/21/429

Abstract

In this paper, we present a semiclassical kinetic approach to tunnelling through potential barriers, which can be applied to the simulation of planar semiconductor devices. The proposed model includes thermionic emission currents at the metal–semiconductor interface as well as tunnelling currents together with the effect of barrier lowering. The considered scattering mechanisms are electron–phonon and electron–impurity interactions. The numerical scheme used is a combination of multicell methods with high-order shock-capturing algorithms. To demonstrate the applicability of the developed method, we present the characteristics of several silicon based Schottky barrier diodes.

1. Introduction

Direct solution methods for the Boltzmann transport equation (BTE) have turned out to be powerful tools to simulate the electron transport in semiconductors. They were successfully applied to study bulk semiconductors [1, 2] as well as diodes [3–7], MESFETs [8] and MOSFETs [9]. However, contact phenomena are often neglected or dealt with by very simple approximations, namely quasi-ohmic and perfectly absorbing boundary conditions. Thus investigations on barrier-controlled devices have hardly been reported, especially under reverse bias conditions. The most common model to describe charge transport across the Schottky barrier is the thermionic emission diffusion (TED) theory by Crowell, Chang and Sze [10]. A unified simulation of Schottky and ohmic contacts is reported in [11]. Monte Carlo (MC) studies dedicated to this problem are presented in [12, 13].

In this paper, we present for the first time approaches to incorporate the thermionic emission current from the metal to the semiconductor and tunnelling currents in both directions into fully discretized deterministic solution methods for the semiclassical BTE. The devised model equations can easily be adapted to other methods which solve the Boltzmann–Poisson system for semiconductors directly. They provide the possibility of treating Schottky contacts with deterministic kinetic models at the same level of physical modelling as some MC methods already do. Concerning the physical details contained in the model, the new approach is more sophisticated than the TED theory but does not provide the complexity of full quantum mechanical models.

The main problem is to find a suitable tradeoff between assumptions usually applied to macroscopic models and a rigorous quantum-mechanical treatment when describing the transport at the barrier by means of the BTE. In most macroscopic models, there are two assumptions involved which in general are only very crude approximations: first, the electrons are considered to be in equilibrium and are described by either Boltzmann or Fermi–Dirac distributions. Second, the electrons are treated as quasi-free particles with a parabolic dispersion relation. Both points can be avoided by applying kinetic transport models, as has been shown, for instance, in [7]. From the quantum-mechanical point of view, interference effects as well as tunnelling, reflections and other interface effects must be taken into account at the barrier [14].

Recently, we presented a model which is able to describe the behaviour of Schottky barrier diodes (SBD) under forward bias [17]. To extend the applicability to reverse bias, it is necessary to incorporate the thermionic emission from the metal to the semiconductor as well as tunnelling effects into the kinetic model. Consequently, a semiclassical description of the quantum mechanical tunnelling process must be developed. For this purpose, we need transition probabilities, which are obtained by applying the WKB approximation [15, 16]. Furthermore, conservation laws for the energy and certain components of the electron wave-vector must be addressed to

describe the final states of the electrons after the tunnelling process correctly.

The paper is organized as follows. In section 2, we introduce the kinetic equations and relevant scattering processes. The discretized model equations are derived in section 3. Their application to device simulation is demonstrated in section 4. Finally, we present the conclusion in section 5.

2. Physical model

On a kinetic level all information about the electron gas is given by the seven-dimensional electron distribution function $f(\boldsymbol{k}, \boldsymbol{x}, t)$, where $\boldsymbol{k} \in \mathbb{R}^3$ denotes the quasi-momentum, $\boldsymbol{x} \in \mathbb{R}^3$ is the position and t time. We assume the following non-parabolic, spherically symmetric dispersion relation for the conduction band electrons of Si:

$$\gamma(\varepsilon) := \varepsilon(1 + \alpha\varepsilon) = \frac{\hbar^2}{2m^*}k^2. \tag{1}$$

Here, m^* is the effective mass, α the non-parabolicity factor and $k = |\boldsymbol{k}|$. Consequently, the group velocity and density of states are given by

$$|v(\boldsymbol{k})| = v(\varepsilon) = \frac{1}{\hbar}\left|\frac{\partial\varepsilon(\boldsymbol{k})}{\partial\boldsymbol{k}}\right| = \frac{1}{\gamma'(\varepsilon)}\sqrt{\frac{2\gamma(\varepsilon)}{m^*}}, \tag{2}$$

$$\mathcal{D}(\varepsilon) = k^2\frac{\mathrm{d}\varepsilon}{\mathrm{d}k} = \frac{1}{2\pi^2}\left(\frac{2m^*}{\hbar^2}\right)^{3/2}\gamma'(\varepsilon)\sqrt{\gamma(\varepsilon)}. \tag{3}$$

We only consider vertical device layouts, i.e., the doping profile varies only along one space direction labelled by z. Along the other two directions, the device is assumed to fill the whole physical space. Due to these assumptions, the distribution function depends on the variables ε, $\mu := (\boldsymbol{k}/k)\cdot\boldsymbol{e}_z$, z and t only. Here, $\boldsymbol{e}_z$ denotes the unit vector in the z-direction. The time evolution of the distribution function $f(\varepsilon, \mu, z, t)$ is governed by the Boltzmann transport equation (BTE):

$$\frac{\partial f}{\partial t} + \mu v\frac{\partial f}{\partial z} - eE\left[\mu v\frac{\partial f}{\partial\varepsilon} + \frac{1-\mu^2}{\sqrt{2m^*\gamma}}\frac{\partial f}{\partial\mu}\right] = \mathcal{C}[f], \tag{4}$$

where e is the positive elementary charge and the electric field strength $E = -\mathrm{d}\Phi/\mathrm{d}t$ has to be calculated self-consistently by solving the Poisson equation for the potential Φ:

$$\frac{\mathrm{d}^2\Phi}{\mathrm{d}z^2} = \frac{e}{\epsilon}[n(z,t) - n_\mathrm{D}(z)]. \tag{5}$$

In this equation, the semiconductor's permittivity is labelled by ϵ and n_D is the fixed profile of donors. The electron density n can be obtained as the zeroth moment from the electron distribution function by

$$\begin{aligned} n(z,t) &= \frac{2}{8\pi^3}\int \mathrm{d}\boldsymbol{k}\, f(\boldsymbol{k}, z, t) \\ &= \frac{1}{2}\iint \mathrm{d}\varepsilon\,\mathrm{d}\mu\,\mathcal{D}(\varepsilon) f(\varepsilon, \mu, z, t), \end{aligned} \tag{6}$$

where the factor 2 in front of the first integral accounts for the spin degeneracy. The collision term $\mathcal{C}$ represents the change of the distribution function due to various scattering mechanisms Γ. If Fermi's statistics is considered for the electrons, terms of the form $f(\varepsilon', \mu')[1 - f(\varepsilon, \mu)]$ must be included. However,

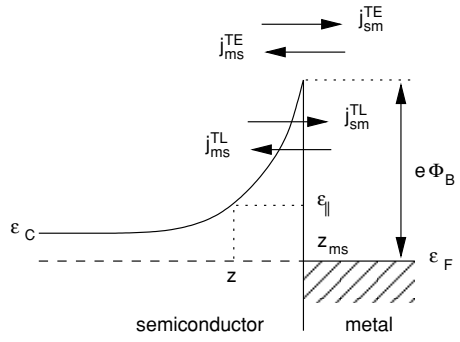

Figure 1. Schematic band diagram of the metal–semiconductor interface.

when dealing with not too high electron densities, i.e. for Fermi energies $\varepsilon_\mathrm{F} < -3k_\mathrm{B}T$ [18], the low density approximation can be applied by supposing $1 - f(\varepsilon, \mu) \approx 1$. For the present band structure, e.g., for a doping of 10^{17} cm^{-3}, the Fermi energy is given by $\varepsilon_\mathrm{F} \approx -4k_\mathrm{B}T$ (which corresponds to a maximum relative error in the order of 0.01 between the Fermi–Dirac distribution and a Boltzmann distribution with the same Fermi energy). Therefore the low density approximation is well applicable and the scattering terms are given by

$$\begin{aligned} \mathcal{C}[f] = \sum_\Gamma \int \mathrm{d}\boldsymbol{k}'[&P^\Gamma(\boldsymbol{k}', \boldsymbol{k}) f(\varepsilon', \mu', z, t) \\ &- P^\Gamma(\boldsymbol{k}, \boldsymbol{k}') f(\varepsilon, \mu, z, t)]. \end{aligned} \tag{7}$$

In the present case, we consider the interaction of the electron gas with a phonon background characterized by a fixed temperature T. The transition rate for acoustic phonon scattering (AP) from state $\boldsymbol{k}$ to $\boldsymbol{k}'$ is given by

$$P^\mathrm{AP}(\boldsymbol{k}, \boldsymbol{k}') = \frac{k_\mathrm{B}T\,\Xi^2}{4\pi^2\hbar\rho u^2}\delta[\varepsilon(\boldsymbol{k}') - \varepsilon(\boldsymbol{k})], \tag{8}$$

where Ξ is the deformation potential, u denotes the average sound velocity and ρ the mass density. Inelastic scattering with non-polar optical phonons (OP) is described by

$$\begin{aligned} P^\mathrm{OP}(\boldsymbol{k}, \boldsymbol{k}') = \frac{D^2}{8\pi^2\rho\omega_\mathrm{op}}\{&N_\mathrm{op}\delta[\varepsilon(\boldsymbol{k}') - \varepsilon(\boldsymbol{k}) - \hbar\omega_\mathrm{op}] \\ &+ (N_\mathrm{op}+1)\delta[\varepsilon(\boldsymbol{k}) - \varepsilon(\boldsymbol{k}) + \hbar\omega_\mathrm{op}]\}, \end{aligned} \tag{9}$$

where D is the deformation field. The occupation number of phonons with the energy $\hbar\omega_\mathrm{op}$ is given by the Bose–Einstein distribution $N_\mathrm{op} = [\exp(\hbar\omega_\mathrm{op}/k_\mathrm{B}T) - 1]^{-1}$. Additionally, we consider ionized impurity scattering (IMP) which is characterized by

$$P^\mathrm{IMP}(\boldsymbol{k}, \boldsymbol{k}') = \frac{N_\mathrm{I}}{\hbar}\left(\frac{e^2}{2\pi\epsilon}\right)^2\frac{\delta[\varepsilon(\boldsymbol{k}') - \varepsilon(\boldsymbol{k})]}{\left(L_\mathrm{D}^{-2} + |\boldsymbol{k} - \boldsymbol{k}'|^2\right)^2} \tag{10}$$

with the impurity concentration N_I and the screening length $L_\mathrm{D} = (\epsilon k_\mathrm{B}T/e^2N_\mathrm{I})^{1/2}$.

At the metal–semiconductor interface, we must take into account four contributions to the carrier transport, as can be seen in figure 1. Electrons which reach the interface from the semiconductor side at z_ms are absorbed by the metal and constitute the current $j^\mathrm{TE}_\mathrm{sm}$. In the opposite direction, only electrons with an energy $\hat{\varepsilon}_\parallel$ due to the motion parallel to the diode principle axis (i.e., perpendicular to the interface),

which surmounts the barrier $\varepsilon_F + e\Phi_B$, contribute to the thermal current j_{ms}^{TE}. Moreover, electrons may tunnel from the silicon to the metal and vice versa with a certain probability P_T, leading to the tunnel currents j_{sm}^{TL} and j_{ms}^{TL}, respectively.

The thermal current from the semiconductor to the metal can be approximated by assuming perfect absorbing boundary conditions for the outflowing electrons, as we have shown in [7], and is given by

$$\left|j_{sm}^{TE}(t)\right| = \frac{1}{2}\int_0^\infty\int_0^1 \mathrm{d}\varepsilon\,\mathrm{d}\mu\,\mu v(\varepsilon)\mathcal{D}(\varepsilon) f(\varepsilon,\mu,z_{ms},t). \quad (11)$$

By assuming that the distribution function in the metal is always in equilibrium described by a Fermi–Dirac distribution f_m, the thermal emission current from the metal into the semiconductor is constant and can be written as

$$\left|j_{ms}^{TE}\right| = A^* T^2 \exp\left(-\frac{e\Phi_B}{k_B T}\right), \qquad A^* = \frac{m_R k_B^2}{2\hbar^3\pi^2} \quad (12)$$

with an effective Richardson constant A^* [19], which corresponds to an effective electron mass m_R. On a microscopic level, this current can be obtained by

$$j_{ms}^{TE} = \frac{1}{4\pi^3}\int \mathrm{d}\hat{\boldsymbol{k}}\, v_{\parallel,m}(\hat{\boldsymbol{k}}) f_m(\hat{\varepsilon})\Theta[-v_{\parallel,m}(\hat{\boldsymbol{k}})]\Theta(\hat{\varepsilon}_\parallel - \hat{\varepsilon}_B), \quad (13)$$

where we assume a parabolic dispersion relation $\hat{\varepsilon} = \hbar^2/(2\hat{m})\hat{k}^2$ with the effective mass $\hat{m}$ in the metal and $v_{\parallel,m}$ is the component of the velocity normal to the interface. The first Heaviside step function takes into account that the electrons contributing to j_{ms}^{TE} flow from the right to the left side (cf figure 1). The second one ensures that only electrons contribute which have enough energy to surmount the barrier. Here $\hat{\varepsilon}_B$ denotes the energy difference from the bottom of the conduction band of the metal to the top of the barrier. This current can be generalized by defining the flux of arbitrary macroscopic quantities $\mathcal{G}(z,t)$ in the semiconductor, which are determined by a microscopic property $g(\boldsymbol{k})$ via

$$\mathcal{G}(z,t) = \frac{2}{8\pi^3}\int \mathrm{d}\boldsymbol{k}\, g(\boldsymbol{k}) f(\boldsymbol{k},z,t). \quad (14)$$

For such a quantity, the corresponding in-flux at the metal–semiconductor interface is given in analogy to (13) by

$$j_{g,ms}^{TE} = \frac{1}{4\pi^3}\int \mathrm{d}\hat{\boldsymbol{k}}\, g(\boldsymbol{k}) v_{\parallel,m}(\hat{\boldsymbol{k}}) f_m(\hat{\varepsilon})\Theta[-v_{\parallel,m}(\hat{\boldsymbol{k}})]\Theta(\hat{\varepsilon}_\parallel - \hat{\varepsilon}_B). \quad (15)$$

It should be noted that a distinction between metal coordinates $\hat{\boldsymbol{k}}$ and semiconductor coordinates $\boldsymbol{k}$ must be made, because the electron wave vector changes when an electron passes the interface. Due to the symmetry with respect to the azimuthal angle and the definitions (2) and (3) of the velocity and DOS for a parabolic band-structure, this integral can be written as

$$j_{g,ms}^{TE} = \frac{\hat{m}}{\hbar^3\pi^2}\int_{\hat{\varepsilon}_B}^\infty\int_{-1}^0 \mathrm{d}\hat{\varepsilon}\,\mathrm{d}\hat{\mu} g(\varepsilon,\mu)\hat{\varepsilon}\hat{\mu} f_m(\hat{\varepsilon})\Theta(\hat{\varepsilon}_\parallel - \hat{\varepsilon}_B). \quad (16)$$

To transform the pair $(\hat{\varepsilon},\hat{\mu})$ on the metal side to the pair (ε,μ) on the semiconductor side, we must consider that the total energy and the components of the wave vector normal to the diodes principle axis are conserved [20]: $\varepsilon + \hat{\varepsilon}_B = \hat{\varepsilon}$ and $k_\perp^2 = \hat{k}_\perp^2$. Moreover, we assume a constant effective mass m_R according to the Richardson constant next to the interface. By combining these assumptions with the two dispersion relations in the metal and the semiconductor, we find

$$\varepsilon = \hat{\varepsilon} - \hat{\varepsilon}_B \qquad \text{and} \qquad \mu^2 = \frac{k^2 - k_\perp^2}{k^2} = 1 - \frac{\hat{\varepsilon} - \hat{\varepsilon}_\parallel}{\gamma(\varepsilon)}. \quad (17)$$

With these relations, the generalized current can be written as

$$j_{g,ms}^{TE} = \frac{m_R}{\hbar^3\pi^2}\int_0^\infty\int_{-1}^0 \mathrm{d}\varepsilon\,\mathrm{d}\mu g(\varepsilon,\mu)\gamma(\varepsilon) \times \mu f_m(\varepsilon + \hat{\varepsilon}_B)\Theta[|\mu| - \mu_m(\varepsilon)] \quad (18)$$

with $\mu_m(\varepsilon) = \sqrt{1 - \varepsilon/\gamma(\varepsilon)}$, where the restriction of $\hat{\varepsilon}_\parallel$ has been transformed into a restriction of μ.

To describe the tunnelling currents, the tunnelling probability P_T is obtained by applying the WKB approximation [16]:

$$P_T[\hat{\varepsilon}_\parallel(z)] = \exp\left\{-2\int_z^{z_{ms}} \mathrm{d}z'\kappa_T(z)\right\}, \qquad \kappa_T(z) := \frac{1}{\hbar}\sqrt{2m^*[\varepsilon_C(z') - \hat{\varepsilon}_\parallel(z)]}, \quad (19)$$

where $\hat{\varepsilon}_\parallel(z)$ and z_{ms} are defined in figure 1. The bottom of the conduction band is determined by the electric potential: $\varepsilon_C := -e\Phi(z)$. In this case, the bottom of the conduction band in the metal must be considered as the reference of zero potential. This approximation does not take into account reflections at the barrier and surface states but has been successfully applied in many applications. However, it remains to be clarified if the main assumption of a slowly varying potential of the WKB approximation is valid for the considered device set-ups. This is the case if $|\mathrm{d}\kappa/\mathrm{d}x| \ll \kappa^2$ [15], which can be expressed as

$$\frac{\hbar m^* eE}{[2m^*(\varepsilon_C - \hat{\varepsilon}_\parallel)]^{3/2}} \ll 1. \quad (20)$$

To model the tunnelling current from the metal into the semiconductor, we observe that in analogy to (16) the relation

$$j_{g,ms}^{TL} = \frac{\hat{m}}{\hbar^3\pi^2}\int_0^\infty\int_{-1}^0 \mathrm{d}\hat{\varepsilon}\,\mathrm{d}\hat{\mu} g(\varepsilon,\mu)\hat{\varepsilon}\hat{\mu} f_m(\hat{\varepsilon}) \times P_T(\hat{\varepsilon}_\parallel)\Theta(\hat{\varepsilon}_B - \hat{\varepsilon}_\parallel) \quad (21)$$

holds for the generalized tunnelling current. The sign of the argument of the Heaviside step function is changed compared to (16), because only electrons which have not enough energy to surmount the barrier contribute to the tunnelling current. Additionally, the tunnelling probability P_T has been considered. To perform the variable transformation from $(\hat{\varepsilon},\hat{\mu})$ to (ε,μ), we again stress the conservation of total energy. To obtain the second condition, it should be noted that the tunnelling depth in the framework of the WKB approximation is defined as the distance between the two classical turning points. Therefore the component of the wave vector normal to the interface must vanish after tunnelling: $k_z = 0$ [21]. It should also be noted that the momentum is not conserved in this model, because only particles which actually tunnel through the barrier are considered. To prove momentum conservation, one must consider transmission and reflection together. By splitting the energy in parallel and normal components and keeping in mind that $\hat{\varepsilon}_\parallel$ is transformed

into potential energy during the tunnelling process, the current can be written as

$$j_{\mathrm{g,ms}}^{\mathrm{TL}} = \frac{\hat{m}}{2\hbar^3\pi^2}\int_0^\infty\int_0^{\hat{\varepsilon}_\mathrm{B}} \mathrm{d}\varepsilon\,\mathrm{d}\hat{\varepsilon}_\parallel g(\varepsilon,0) f_\mathrm{m}(\hat{\varepsilon}) P_\mathrm{T}(\hat{\varepsilon}_\parallel). \tag{22}$$

Here $\varepsilon = \hat{\varepsilon}_\perp = \hat{\varepsilon} - \hat{\varepsilon}_\parallel$. Finally, the generalized current can also be written as

$$j_{\mathrm{g,ms}}^{\mathrm{TL}} = \frac{\hat{m}}{2\hbar^3\pi^2}\int_0^\infty\int_{-1}^1\int_0^{\hat{\varepsilon}_\mathrm{B}} \mathrm{d}\varepsilon\,\mathrm{d}\mu\,\mathrm{d}\hat{\varepsilon}_\parallel g(\varepsilon,\mu) \times f_\mathrm{m}(\hat{\varepsilon}) P_\mathrm{T}(\hat{\varepsilon}_\parallel)\delta(0-\mu). \tag{23}$$

The Schottky barrier height Φ_B plays an important role, because the parameter $\hat{\varepsilon}_\mathrm{B}$ for the different currents at the interface depends on the barrier via $\hat{\varepsilon}_\mathrm{B} = \Phi_\mathrm{B} + \mu_\mathrm{F}$. The chemical potential μ_F in the metal remains constant during the simulation, but the barrier height may vary depending on the electric field E_ms at the interface. Usually, it is decomposed into a static and a field dependent contribution:

$$\hat{\Phi}_\mathrm{B}(E_\mathrm{ms}) = \Phi_\mathrm{B} - \Delta\Phi_\mathrm{B}(E_\mathrm{ms}). \tag{24}$$

One effect which influences the barrier height is the barrier lowering due to the image force, which is given by [22]

$$\Delta\Phi_\mathrm{B}^\mathrm{IF} = \sqrt{\frac{e|E_\mathrm{ms}|}{4\pi\epsilon}}. \tag{25}$$

Another point which must be discussed is that the metal–semiconductor interface is not a perfect heterojunction. For example, dipoles and surface states may be present. The effect of dipoles at the interface layer is described by [22, 23]:

$$\Delta\Phi_\mathrm{B}^\mathrm{DP} = \alpha_\mathrm{B} E_\mathrm{ms}, \tag{26}$$

where α_B is an empirical parameter. Thus the final field-dependent barrier height is given by

$$\hat{\Phi}_\mathrm{B}(E_\mathrm{ms}) = \Phi_\mathrm{B} - \sqrt{\frac{e|E_\mathrm{ms}|}{4\pi\epsilon}} - \alpha_\mathrm{B} E_\mathrm{ms}. \tag{27}$$

It should be noted that the barrier lowering affects only the current from the metal to the semiconductor, because electrostatic effects are already included in the transport equations due to the coupling of the BTE with the Poisson equation.

3. Numerical treatment

The model equations are obtained from the BTE by applying the multicell-WENO method we have presented in [7]. This technique is a combination of the method of weighted residuals [24] and high-order shock capturing algorithms [25]. It is based on a partition of the (ε,μ)-space into cells $B_{\nu\lambda} := I_\nu \times I_\lambda$ with $\nu = 1,\ldots,N_\nu$ and $\lambda = 1,\ldots,N_\lambda$. The energy intervals are defined by $I_\nu = [\varepsilon_{\nu-1},\varepsilon_\nu]$ with $\Delta\varepsilon := \varepsilon_\nu - \varepsilon_{\nu-1} = \hbar\omega_\mathrm{op}/s$, $s \in \mathrm{N}^+$, $\varepsilon_0 = 0$ and $\varepsilon_\mathrm{max} = N_\nu\Delta\varepsilon$. The μ-space is divided into the intervals $I_\lambda = [\mu_{\lambda-1},\mu_\lambda]$ with $\mu_\lambda = \lambda\Delta\mu - 1$ and $\Delta\mu = 2/N_\mu$. In the (ε,μ)-plane, we approximate the product of the distribution function and the density of states $\Psi(\varepsilon,\mu,z,t) := \mathcal{D}(\varepsilon) f(\varepsilon,\mu,z,t)$ by a discontinuous bilinear form

$$\Psi(\varepsilon,\mu,z,t) \approx \sum_{\nu=1}^{N_\nu}\sum_{\lambda=1}^{N_\lambda} \chi_{B_{\nu\lambda}}(\varepsilon,\mu) \times \sum_{\alpha,\beta=0}^{1} P_\nu^\alpha(\varepsilon) P_\lambda^\beta(\mu) \Psi_{\nu\lambda}^{\alpha\beta}(z,t) \tag{28}$$

with the characteristic functions

$$\chi_{B_{\nu\lambda}}(\varepsilon,\mu) = \begin{cases} 1 & \text{if } (\varepsilon,\mu) \in B_{\nu\lambda} \\ 0 & \text{elsewhere,} \end{cases} \tag{29}$$

and the basis functions

$$P_\nu^\alpha(\varepsilon) = \sqrt{\frac{2}{\Delta\varepsilon}} P^\alpha\left[\frac{2}{\Delta\varepsilon}\left(\varepsilon + \frac{\Delta\varepsilon}{2} - \varepsilon_\nu\right)\right], \tag{30}$$

$$P_\lambda^\beta(\mu) = \sqrt{\frac{2}{\Delta\mu}} P^\beta\left[\frac{2}{\Delta\mu}\left(\mu + \frac{\Delta\mu}{2} - \mu_\lambda\right)\right], \tag{31}$$

where $P^{\alpha/\beta}$ are the Legendre polynomials of order α/β. The leading factors and the transformation of the arguments are chosen in a way that the modified Legendre polynomials fulfil the same orthogonality relation as the original Legendre polynomials. By multiplying the BTE (4) by $\mathcal{D}P_\nu^{\alpha'}P_\lambda^{\beta'}$, the products $\mathcal{D}f$ can be replaced by the ansatz (28). By integrating the resulting equations with respect to ε and μ over the cells $B_{\nu\lambda}$, the orthogonality of the basis functions can be exploited yielding the model equations

$$\delta^{\alpha'}\delta^{\beta'}\frac{\partial\Psi_{\nu\lambda}^{\alpha'\beta'}}{\partial t} + \sum_{\alpha,\beta=0}^{1} v_\nu^{\alpha\alpha'}\mu_\lambda^{\beta\beta'}\frac{\partial\Psi_{\nu\lambda}^{\alpha\beta}}{\partial z} + \mathcal{F}_{\nu\lambda}^{\alpha'\beta'}[\Psi] = \mathcal{C}_{\nu\lambda}^{\alpha'\beta'}[\Psi]. \tag{32}$$

We used the abbreviations $\delta^x = 2/(2x+1)$, $v_\nu^{\alpha\alpha'} = \int_{I_\nu} v P_\nu^\alpha P_\nu^{\alpha'}\,\mathrm{d}\varepsilon$ and $\mu_\lambda^{\beta\beta'} = \int_{I_\lambda}\mu P_\lambda^\beta P_\lambda^{\beta'}\,\mathrm{d}\mu$.

The force term in (32) can be written as

$$\begin{aligned}\mathcal{F}_{\nu\lambda}^{\alpha'\beta'}[\Psi] = -eE\Bigg\{&\int_{I_\lambda}\mathrm{d}\mu\left[\mu v\Psi(\varepsilon,\mu)P_\nu^{\alpha'}P_\lambda^{\beta'}\right]_{I_\nu} \\ &+ \int_{I_\nu}\mathrm{d}\varepsilon\left[\frac{1-\mu^2}{\sqrt{2m^*\gamma}}\Psi(\varepsilon,\mu)P_\nu^{\alpha'}P_\lambda^{\beta'}\right]_{I_\lambda} \\ &- \int_{I_\nu}\int_{I_\lambda}\mathrm{d}\varepsilon\,\mathrm{d}\mu\Psi(\varepsilon,\mu) \\ &\times\left[\mu v\frac{\mathrm{d}P_\nu^{\alpha'}}{\mathrm{d}\varepsilon}P_\lambda^{\beta'} + \frac{1-\mu^2}{\sqrt{2m^*\gamma}}P_\nu^{\alpha'}\frac{\mathrm{d}P_\lambda^{\beta'}}{\mathrm{d}\mu}\right]\Bigg\},\end{aligned} \tag{33}$$

where we omitted the dependence of Ψ on z and t. Here, the notation $[u(x)]_I$, $I = [a,b]$ means $[u(x)]_I = u(b) - u(a)$ for arbitrary functions $u(x)$ and $a, b \in \mathbb{R}$. Thus, the first two terms in square brackets must be determined at the borders of two adjacent energy and angular cells, respectively. It should be noted that the ansatz (28) is discontinuous at the borders of the cells and therefore it is not clear, *a priori*, in which cell $\Psi(\varepsilon,\mu)$, represented by (28), must be evaluated. By considering, e.g., the first term in square brackets for ε_ν, either the energy cell with index ν or $(\nu+1)$ is a possible choice for the ansatz. However, to guarantee the stability of the numerical scheme, this choice is governed by a proper upwinding following the characteristics of (4). For the upwinding with respect to ε, the direction is determined by the factor μE and, consequently, the ansatz at the border ε_ν must be evaluated for $\tilde{\nu} = \nu + \sigma_\varepsilon(\mu,E)$, where the offset of the energy-cell index is given by $\sigma_\varepsilon(\mu,E) = \Theta(\mu E)$. Considering the upwinding in μ-direction, we find that for the border μ_λ the ansatz must be taken for $\tilde{\mu} = \mu + \sigma_\mu(E)$ with $\sigma_\mu = \Theta(E)$ since the upwinding is only determined by the sign of the electric field in this case. By taking into account these rules when inserting the ansatz (28) into

(33) and performing the integrations, the force term can be written as

$$\begin{aligned}\mathcal{F}_{\nu\lambda}^{\alpha'\beta'}[\Psi] = -eE \sum_{\alpha,\beta=0}^{1} \{\mu_\lambda^{\beta\beta'}\big[h_{\nu\lambda}^{\varepsilon}\left(\varepsilon_\nu, \sigma_\varepsilon^\lambda\right) \\ - h_{\nu\lambda}^{\varepsilon}\left(\varepsilon_{\nu-1}, \sigma_\varepsilon^\lambda - 1\right) - \tilde{v}_\nu^{\alpha\alpha'}\Psi_{\nu\lambda}^{\alpha\beta}\big] \\ - \gamma_\nu^{\alpha\alpha'}\big[h_{\nu\lambda}^{\mu}(\mu_\lambda, \sigma_\mu) - h_{\nu\lambda}^{\mu}(\mu_{\lambda-1}, \sigma_\mu - 1) \\ - \tilde{\mu}_\lambda^{\beta\beta'}\Psi_{\nu\lambda}^{\alpha\beta}\big]\},\end{aligned} \tag{34}$$

with the symbols $\sigma_\varepsilon^\lambda = \sigma_\varepsilon(\mu_\lambda, E)$, $\tilde{v}_\nu^{\alpha\alpha'} = 2\delta_{\alpha'1}v_\nu^{\alpha 0}/\Delta\varepsilon$, $\tilde{\mu}_\lambda^{\beta\beta'} = 2\delta_{\beta'1}\left(2\delta_{\beta 0} - \mu_\lambda^{\beta 0}\right)/\Delta\mu$ and $\gamma_\nu^{\alpha\alpha'} = \int_{I_\nu}(2m^*\gamma)^{-1/2}P_\nu^\alpha P_\nu^{\alpha'}\,\mathrm{d}\varepsilon$. Here we introduced the numerical fluxes in the ε- and μ-directions, respectively, which are given by

$$h_{\nu\lambda}^{\varepsilon}(\varepsilon, \sigma) = v(\varepsilon)P_\nu^{\alpha'}(\varepsilon)P_{\nu+\sigma}^{\alpha}(\varepsilon)\Psi_{(\nu+\sigma)\lambda}^{\alpha\beta} \tag{35}$$

$$h_{\nu\lambda}^{\mu}(\mu, \sigma) = (1-\mu^2)P_\lambda^{\beta'}(\mu)P_{\lambda+\sigma}^{\beta}(\mu)\Psi_{\nu(\lambda+\sigma)}^{\alpha\beta}. \tag{36}$$

For the collision term, we find the general representation

$$\begin{aligned}\mathcal{C}_{\nu\lambda}^{\alpha'\beta'}[\Psi] &= \sum_\Gamma \mathcal{C}_{\nu\lambda}^{\Gamma,\alpha'\beta'}[\Psi] \\ &= \sum_{\Gamma,\alpha,\beta}\left[\left(\sum_{\lambda'}\mathcal{C}_{\mathrm{G},\nu\lambda\lambda'}^{\Gamma,\alpha\alpha'\beta\beta'}\Psi_{\hat{\nu}_\Gamma(\nu)\lambda'}^{\alpha\beta}\right) - \mathcal{C}_{\mathrm{L},\nu\lambda}^{\Gamma,\alpha\alpha'\beta\beta'}\Psi_{\nu\lambda}^{\alpha\beta}\right].\end{aligned} \tag{37}$$

In the case of elastic scattering events, i.e. AP and IMP, we have no offset of the energy group in the gain term: $\nu_{\mathrm{AP/IMP}}(\nu) = \nu$. The offset for absorption of an optical phonon is given by $\nu_{\mathrm{OP,A}}(\nu) = \nu - s$, while the offset for emission of a phonon reads $\nu_{\mathrm{OP,E}}(\nu) = \nu + s$. By introducing $\hat{\mathcal{D}}(\varepsilon) = \mathcal{D}(\varepsilon)\Theta(\varepsilon)\Theta(\Delta\varepsilon N_\varepsilon - \varepsilon)$, $\mathcal{D}_\nu^{\alpha\alpha'}(\Delta) = \int_{I_\nu}\hat{\mathcal{D}}(\varepsilon+\Delta)P_\nu^\alpha(\varepsilon)P_\nu^{\alpha'}(\varepsilon)\,\mathrm{d}\varepsilon$ and $c_{\mathrm{AP}} = \pi k_{\mathrm{B}}T\,\Xi^2/\hbar\rho u^2$, the constants for acoustic phonon scattering are given by

$$\begin{aligned}\mathcal{C}_{\mathrm{G},\nu\lambda\lambda'}^{\mathrm{AP},\alpha\alpha'\beta\beta'} &= c_{\mathrm{AP}}\Delta\mu\delta_{\beta 0}\delta_{\beta' 0}\mathcal{D}_\nu^{\alpha\alpha'}(0), \\ \mathcal{C}_{\mathrm{L},\nu\lambda}^{\mathrm{AP},\alpha\alpha'\beta\beta'} &= c_{\mathrm{AP}}\delta_{\beta\beta'}\delta^{\beta'}\mathcal{D}_\nu^{\alpha\alpha'}(0).\end{aligned} \tag{38}$$

For optical phonon scattering, the constants read

$$\begin{aligned}\mathcal{C}_{\mathrm{G},\nu\lambda\lambda'}^{\mathrm{OP,A},\alpha\alpha'\beta\beta'} &= c_{\mathrm{OP}}\Delta\mu\delta_{\beta 0}\delta_{\beta' 0}N_{\mathrm{op}}\mathcal{D}_\nu^{\alpha\alpha'}(0), \\ \mathcal{C}_{\mathrm{L},\nu\lambda}^{\mathrm{OP,A},\alpha\alpha'\beta\beta'} &= c_{\mathrm{OP}}\delta_{\beta\beta'}\delta^{\beta'}N_{\mathrm{op}}\mathcal{D}_\nu^{\alpha\alpha'}(\hbar\omega_{\mathrm{op}}),\end{aligned} \tag{39}$$

$$\begin{aligned}\mathcal{C}_{\mathrm{G},\nu\lambda\lambda'}^{\mathrm{OP,A},\alpha\alpha'\beta\beta'} &= c_{\mathrm{OP}}\Delta\mu\delta_{\beta 0}\delta_{\beta' 0}(N_{\mathrm{op}}+1)\mathcal{D}_\nu^{\alpha\alpha'}(0), \\ \mathcal{C}_{\mathrm{L},\nu\lambda}^{\mathrm{OP,A},\alpha\alpha'\beta\beta'} &= c_{\mathrm{OP}}\delta_{\beta\beta'}\delta^{\beta'}(N_{\mathrm{op}}+1)\mathcal{D}_\nu^{\alpha\alpha'}(-\hbar\omega_{\mathrm{op}}),\end{aligned} \tag{40}$$

with $c_{\mathrm{OP}} = \pi D^2/2\rho\omega_{\mathrm{op}}$. Finally, the collision constants for impurity scattering equal

$$\begin{aligned}\mathcal{C}_{\mathrm{G},\nu\lambda\lambda'}^{\mathrm{IMP},\alpha\alpha'\beta\beta'} &= c_{\mathrm{IMP}}\int_{I_\nu}\mathrm{d}\varepsilon\int_{I_\lambda}\mathrm{d}\mu\int_{I_{\lambda'}}\mathrm{d}\mu'\mathcal{D}(\varepsilon)P_\nu^\alpha(\varepsilon)P_\nu^{\alpha'}(\varepsilon) \\ &\quad\times P_\lambda^{\beta'}(\mu)P_{\lambda'}^{\beta}(\mu')\mathcal{K}(\varepsilon,\mu,\mu'), \\ \mathcal{C}_{\mathrm{L},\nu\lambda}^{\mathrm{IMP},\alpha\alpha'\beta\beta'} &= c_{\mathrm{IMP}}\int_{I_\nu}\mathrm{d}\varepsilon\int_{I_\lambda}\mathrm{d}\mu\int_{-1}^{1}\mathrm{d}\mu'\mathcal{D}(\varepsilon)P_\nu^\alpha(\varepsilon)P_\nu^{\alpha'}(\varepsilon) \\ &\quad\times P_\lambda^{\beta'}(\mu)P_\lambda^{\beta}(\mu)\mathcal{K}(\varepsilon,\mu,\mu'),\end{aligned} \tag{41}$$

where $c_{\mathrm{IMP}} = \pi\mathrm{e}^4N_{\mathrm{I}}/2\hbar\epsilon^2$ and the scattering kernel is given by

$$\begin{aligned}\mathcal{K}(\varepsilon,\mu,\mu') &= \left[L_{\mathrm{D}}^{-2} + \frac{4m^*}{\hbar^2}\gamma(\varepsilon)(1-\mu\mu')\right] \\ &\quad\times\left\{L_{\mathrm{D}}^{-4} + \frac{8m^*}{\hbar^2}L_{\mathrm{D}}^{-2}\gamma(\varepsilon)(1-\mu\mu')\right. \\ &\quad\left.+\left[\frac{4m^*}{\hbar^2}\gamma(\varepsilon)(\mu-\mu')\right]^2\right\}^{-3/2}.\end{aligned} \tag{42}$$

To deal with the spatial dependence, we consider $\Psi_{\nu\lambda}^{\alpha\beta}(z,t)$ on a mesh $\{z_i, \Delta z_i\}, i = 1,\ldots,N_z$, where the grid points are located in the centre of the cells and label the coefficients at the grid points with $\Psi_{\nu\lambda i}^{\alpha\beta} := \Psi_{\nu\lambda}^{\alpha\beta}(z_i,t)$. Further, we label the positions of the left and right boundary of each cell i with $z_{i-1/2}$ and $z_{i+1/2}$, respectively. We treat the spatial operator in (32) by means of a conservative flux formulation:

$$\sum_{\alpha,\beta=0}^{1}\left\{v_\nu^{\alpha\alpha'}\mu_\lambda^{\beta\beta'}\frac{\partial\Psi_{\nu\lambda}^{\alpha\beta}}{\partial z}\right\}_{z=z_i} = \frac{1}{\Delta z_i}\left(\overline{h}_{\nu\lambda i}^{\alpha'\beta'}[\Psi] - \underline{h}_{\nu\lambda i}^{\alpha'\beta'}[\Psi]\right), \tag{43}$$

where, in general, the fluxes $\overline{h}$ and $\underline{h}$ are obtained by a WENO approximation [25, 6]. In this case, we apply the third order WENO approximation for non-uniform grids presented in [7]. Based on the generalized current

$$j_{\mathrm{g}}(z,t) = \frac{1}{2}\int_0^{\varepsilon_{\max}}\int_{-1}^{1}\mathrm{d}\varepsilon\,\mathrm{d}\mu\,g(\varepsilon,\mu)\mathcal{D}(\varepsilon)\mu v(\varepsilon)f(\varepsilon,\mu,z,t) \tag{44}$$

in analogy to (18), we find that the numerical fluxes $\overline{h}_{\nu\lambda i}^{\alpha'\beta'}$ are proportional to the contributions to the generalized currents with $\tilde{g} = P_\nu^{\alpha'}P_\lambda^{\beta'}$ in the different energy-angle cells $B_{\nu\lambda}$ at $z_{i+1/2}$. Therefore, the current can be written as

$$j_{\tilde{\mathrm{g}}}(z_{i+1/2}) = \frac{1}{2}\sum_{\nu,\lambda}\overline{h}_{\nu\lambda i}^{\alpha'\beta'}. \tag{45}$$

If we consider the metal–semiconductor interface, which is also the cell boundary $z_{N_z+1/2}$, all electrons in the angular cells with $\lambda > N_\lambda/2$, i.e. $\mu_\lambda > 0$, flow out of the device and constitute the current $j_{\mathrm{sm}}^{\mathrm{TE}}$. In this case, the corresponding fluxes $\overline{h}_{\nu\lambda N_z}^{\alpha'\beta'}$ can be modelled by absorbing boundary conditions for the WENO reconstruction procedure, as we have pointed out in [17]. In the case of $\mu_\lambda < 0$, the fluxes are determined by the current $j_{\mathrm{g,ms}}^{\mathrm{TE}}$ and are therefore given by (18):

$$\begin{aligned}\overline{h}_{\nu\lambda N_z}^{\alpha'\beta'} &= \frac{2m_{\mathrm{R}}}{\hbar^3\pi^2}\int_{I_\nu}\int_{I_\lambda}\mathrm{d}\varepsilon\,\mathrm{d}\mu\,P_\nu^{\alpha'}(\varepsilon)P_\lambda^{\beta'}(\mu)\gamma(\varepsilon) \\ &\quad\times\mu f_{\mathrm{m}}(\varepsilon+\hat{\varepsilon}_{\mathrm{B}})\Theta[|\mu| - \mu_{\mathrm{m}}(\varepsilon)].\end{aligned} \tag{46}$$

In order to derive the model equations for tunnelling from the metal into the semiconductor, we follow a similar argumentation for the generalized tunnelling current (23). However, we must additionally consider that the integration limits for $\hat{\varepsilon}_\parallel$ depend on the position z of the considered cell i via the potential Φ (cf figure 1). In addition, we assume that the pole of the Dirac delta distribution lies completely in cells with $\lambda_{\mathrm{T}} = N_\mu/2$, i.e. in a cell with negative angles, which

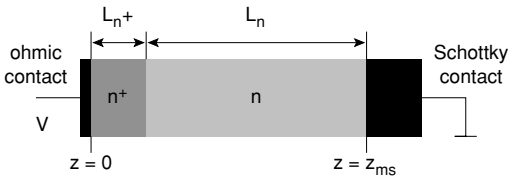

Figure 2. General layout of the simulated SBDs.

Table 1. Material parameters of Si for the numerical calculations.

Quantity	Value	Unit	Quantity	Value	Unit
m^*/m_0	0.26	–	T	300	K
ϵ_0	8.854×10^{-12}	F m−1	ϵ	11.7 ϵ_0	F m−1
α	0.5	eV^{-1}	$\hbar\omega_{op}$	63	meV
Ξ	9.0	eV	D	1.14×10^9	eV cm^{-1}
ρ	2.33	g cm^{-3}	u	9.04×10^5	cm s^{-1}

means that the tunnelling current flows from the right- to the left-hand side. Considering these assumptions, we obtain the tunnelling fluxes

$$\overline{h}^{\alpha'\beta',\mathrm{TL}}_{\nu\lambda N_z} = \frac{m_\mathrm{R}}{\hbar^3\pi^2}\sqrt{\frac{2}{\Delta\mu}}\delta_{\lambda,\lambda_\mathrm{T}}\int_{I_\nu}\int_{\hat{\varepsilon}_\parallel(z_{i-1/2})}^{\hat{\varepsilon}_\parallel(z_{i+1/2})} \mathrm{d}\varepsilon\,\mathrm{d}\mu\,P_\nu^{\alpha'}(\varepsilon) \times f_\mathrm{m}(\varepsilon+\hat{\varepsilon}_\mathrm{B})P_\mathrm{T}(\hat{\varepsilon}_\parallel). \quad (47)$$

Finally, we implement tunnelling from the semiconductor into the metal by replacing the common flux conservative relation $\underline{h}_{i+1} = \overline{h}_i$ with

$$\underline{h}^{\alpha'\beta'}_{\nu\lambda(i+1)} = \begin{cases} \overline{h}^{\alpha'\beta'}_{\nu\lambda i} & \text{for downwinding } \lambda \leqslant N_\lambda/2 \\ \{1 - P_\mathrm{T}[\hat{\varepsilon}_\parallel(z_i)]\}\overline{h}^{\alpha'\beta'}_{\nu\lambda i} & \text{for upwinding } \lambda > N_\lambda/2. \end{cases} \quad (48)$$

4. Numerical results

In this section, we apply the developed model equations to simulate Schottky barrier diodes with metal–Si interfaces. The material parameters, which remain the same throughout all simulations, are listed in table 1. Unless stated otherwise, we use an effective Richardson constant $A^* = 112$ $\mathrm{Acm^{-2}\,K^{-2}}$ for silicon. To treat impurity scattering, we assume that the impurity concentration equals the doping profile in all simulations, i.e. $N_\mathrm{I} = N_\mathrm{I}(z) = n_\mathrm{D}(z)$. The general layout of the simulated SBDs is shown in figure 2. We assume a high doped n^+ region to establish the ohmic contact next to the active n region with the metal–semiconductor interface.

The first device we consider is a SBD with a $ZrSi_2$/n-Si contact with a total length of 1 μm ($L_{n^+} = 0.2$ μm and $L_n = 0.8$ μm). The high and low doping concentrations are given by $n^+ = 10^{17}$ $\mathrm{cm^{-3}}$ and $n = 10^{16}$ $\mathrm{cm^{-3}}$, respectively. For the discretization we take the grid sizes $N_\nu = 40$ (with $s = 2$), $N_\lambda = 4$ and $N_z = 130$. The cell sizes for the spatial grid are $\Delta z_i = 10$ nm, $1 \leqslant i \leqslant 70$ and $\Delta z_i = 5$ nm, $70 < i \leqslant 130$. The contact parameters are $e\Phi_\mathrm{B} = 0.55$ eV and $\alpha_\mathrm{B} = 1.5$ nm [22]. Figure 3 shows the current–voltage characteristics of this device under reverse bias for several model situations. It can be seen that the out-tunnelling plays only a minor role

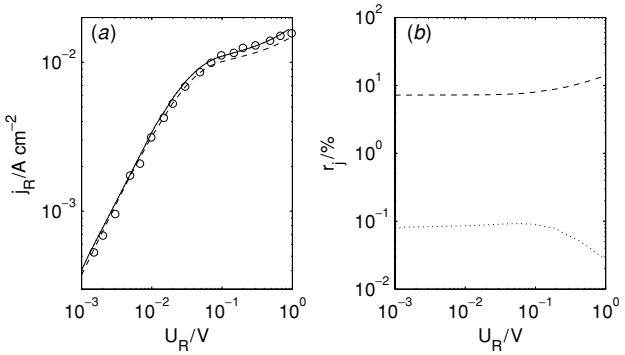

Figure 3. (*a*) Reverse current–voltage characteristics of the $ZrSi_2$/n-Si diode by including barrier lowering as well as full tunnelling (——), in-tunnelling only (· · · · · ·, coincides with ——) and no tunnelling (- - - -). Experimental data (○) are given as in [22]. (*b*) Deviations of the cases with in-tunnelling only (· · · · · ·) and no tunnelling (- - - -) with respect to full tunnelling.

with a contribution of less than 0.1% to the overall current. The in-tunnelling contributes in the order of 10%. Here the relative error r_j of the current j with respect to a reference j_ref is given by $r_j = |j - j_\mathrm{ref}|/j_\mathrm{ref}$. A comparison with experimental data [22] indicates that the tunnelling current is slightly overestimated by the WKB approximation. It shows that the tunnelling probability differs significantly from zero only in the cell adjacent to the metal–semiconductor contact for the used discretization with respect to z. Unfortunately, a numerical investigation of the WKB validity criterion equation (20) in this space-cell reveals that the application of the WKB method is questionable. However, the potential in this region can be very well approximated by a linear potential and thus an exact solution of the Schrödinger equation in the form of Airy functions is possible. Following the argumentation for the derivation of the WKB tunnelling probability [15], we obtain a tunnelling probability $T = 0.38$ between the interface and the first point inside the diode for an applied reverse bias of 1 V. The probability due to WKB is $T = 0.43$, which is a deviation of 13%. By considering the contribution of the tunnelling current to the total current, the error due to the WKB approximation is less than 3%. It must be stated that this estimation accounts for the difference between the approximated WKB solution and exact Airy functions only. The definition of the tunnelling probability and the influence of reflections in the barrier region cannot be treated in a full quantum mechanical manner [26], since in our approach all electrons in classically allowed regions are governed by the BTE.

The dependence of the thermionic currents and barrier height on the applied voltage is illustrated in figure 4. It should be noted that the current from the metal to the semiconductor varies only because the barrier height changes due to the barrier lowering. The variation of the current from the semiconductor to the metal is independent of this barrier lowering. The effect of barrier lowering on the overall current is studied in figure 5. Here we observe that already the influence of the dipole lowering equals the influence of the overall tunnelling current. The full influence of around 50% and more of the barrier lowering exceeds the one of tunnelling by a factor of 5. In figure 6, we assume $A^* = 156$ $\mathrm{Acm^{-2}\,K^{-2}}$ to perform

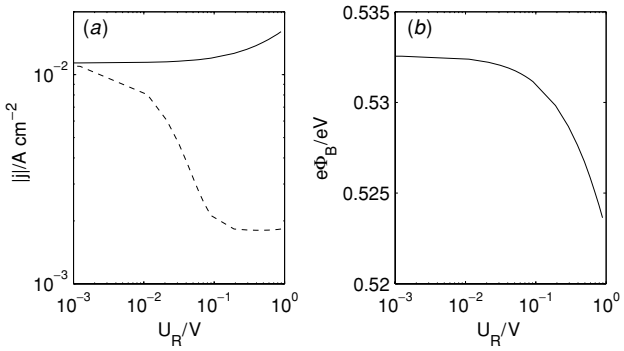

Figure 4. (a) Thermionic currents $|j_{ms}^{TE}|$(——) and $|j_{sm}^{TE}|$(- - - -) at the metal–semiconductor interface as a function of the applied reverse bias. (b) Dependence of the barrier height $e\Phi_B$ on the reverse bias.

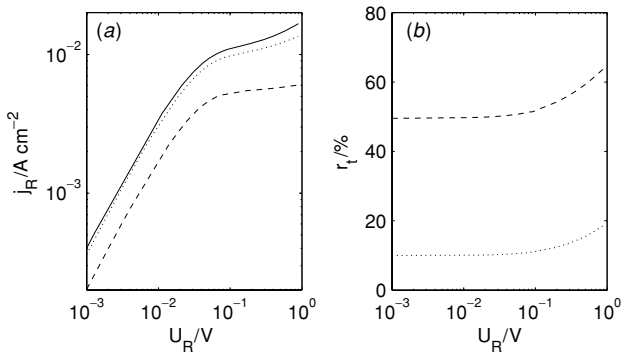

Figure 5. (a) Reverse current–voltage characteristics of the $ZrSi_2$/n-Si diode including tunnelling and barrier lowering (——), barrier lowering with $\alpha_B = 0$ nm (· · · · · ·) and no barrier lowering (- - - -). (b) Deviation of the current in the cases with reduced barrier lowering with respect to the case with full barrier lowering.

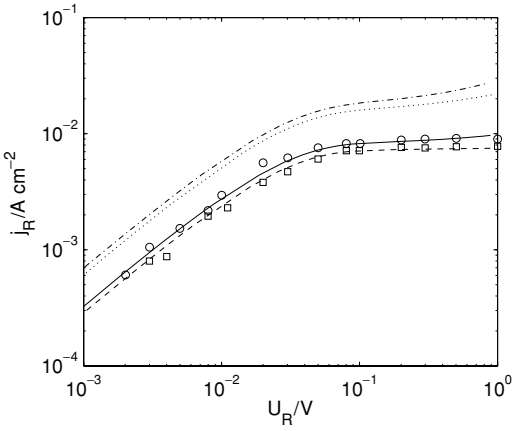

Figure 6. Reverse current–voltage characteristics of the $ZrSi_2$/n-Si diode for $A^* = 156$ Acm^{-2} K^{-2}. The results are obtained without barrier lowering for the case with tunnelling (—— and ○) and without tunnelling (- - - - and □), where the symbols are the corresponding MC results [13]. By including barrier lowering, higher currents were observed where (— · —) refers to the case with tunnelling and (· · · · · ·) to the case without tunnelling.

comparisons with MC data [13] where barrier lowering is not considered. As can be seen, both methods yield the same currents due to tunnelling. If, however, barrier lowering

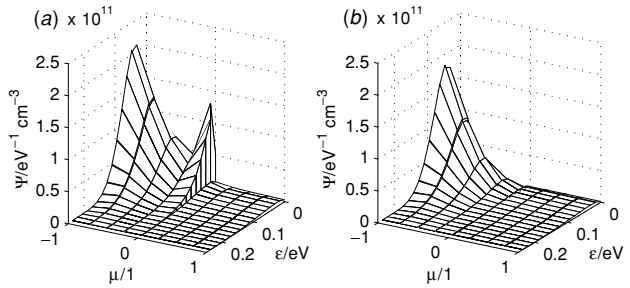

Figure 7. Electron distribution Ψ versus energy ε and angle μ at the metal–semiconductor interface with tunnelling (a) and without tunnelling (b) for an applied reverse bias of $U_R = 1$ V.

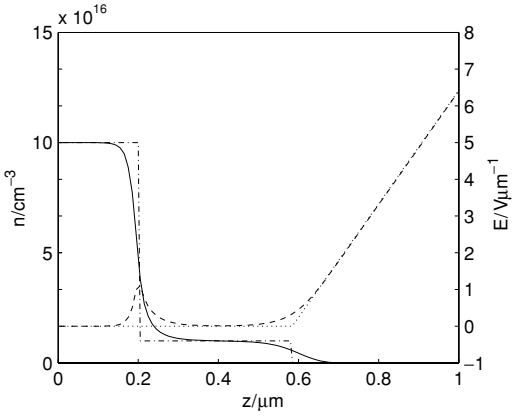

Figure 8. Comparison of the simulated particle density n(——) and electric field E(- - - -) with the corresponding macroscopic results (— · —) and (· · · · · ·), respectively.

is considered, it shows that the used effective Richardson constant overestimates the current by a factor of 2.

The effect of tunnelling on the distribution function at the metal–semiconductor interface is shown in figure 7. In the present case, the applied reverse bias is $U_R = 1$ V. If tunnelling is present, we observe a peak at $\mu = 0$ which is caused by the Kronecker delta in equation (47). This means that all electrons which tunnel from the metal to the semiconductor occupy a state at $\mu = 0$ after tunnelling since all the energy due to the motion parallel to the z-direction is transferred into potential energy in the WKB model. The comparison of the obtained steady state particle density and electric field profiles with those of the macroscopic theory [19] is presented in figure 8. We observe a good agreement of the results concerning the width of the depletion layer and the electric field strength at the metal–semiconductor interface. Differences arise at the junctions of the n^+- and n-regions as well as of the n- and depletion-regions, because the full depletion approximation is used to derive the macroscopic model. Our results show that such a discontinuity of the particle density (and consequently the sharp bend of the electric field) is not a very good approximation since we observe a region of a length of about 0.05 μm where the particle density varies smoothly between the depletion- and n-doped regions.

The next device considered is a SBD with a RhSi/n-Si contact [22]. The two doping regions are given by ($n^+ = 10^{17}$ cm^{-3}, $L_{n^+} = 0.2$ μm) and ($n = 3.5 \times 10^{15}$ cm^{-3},

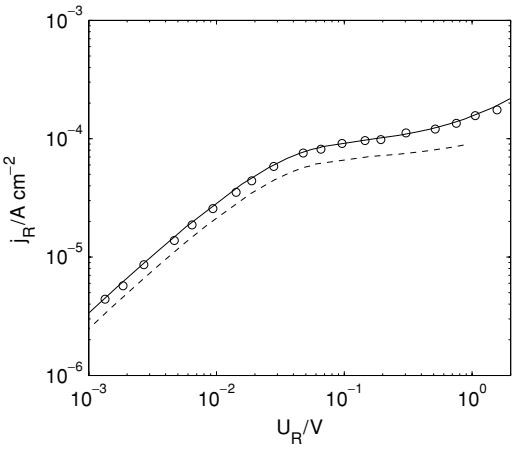

Figure 9. Reverse current–voltage characteristics of the RhSi/n-Si diode with (——) and without (- - - -) inclusion of barrier lowering due to dipoles according to equation (26). The circles are measured results [22].

$L_n = 1.8\,\mu$m). Although this device is not as long as the one considered in [22] to speed up the calculation, comparisons can be made, since the characteristics are mainly influenced by the depletion region. In the considered set-up and for the applied voltages, the distance from the n^+ region to the depletion region is always greater than 0.3 μm. The computational grid is defined by ($N_\nu = 40$, s $= 2$, $N_\lambda = 4$, $N_z = 300$) with $\Delta z_i = 10$ nm, $1 \leqslant i \leqslant 170$ and $\Delta z_i = 2$ nm, $170 < i \leqslant 320$. For the contact, we assume $e\Phi_B = 0.68$ eV and $\alpha_B = 3.5$ nm. The resulting current–voltage characteristic is shown in figure 9. As can be seen, the barrier lowering due to dipoles plays a much more important role for the RhSi contact than for the $ZrSi_2$ contact. If this effect is taken into account, we obtain a very good agreement with experimental data.

5. Conclusions

In this paper, we present a direct solution method for the coupled Boltzmann–Poisson system in semiconductors which accounts for metal–semiconductor interface effects. The method is applied to simulate Schottky barrier diodes. The results show a good agreement with experimental data as well as data obtained with other numerical methods. Our simulations confirm that the device characteristics strongly depend on barrier lowering, which is caused by the image force and dipoles at the interface. To treat the tunnelling through the Schottky barrier, we use the WKB method. Although the application of this approximation for non-slowly varying potentials is questionable, we observe very good agreements of the simulated I–V curves with the measured ones. This is the case because the overall influence of the error due to WKB is estimated to be less than 3%. Therefore the Boltzmann–Poisson solver provides a very accurate description of electron dynamics in devices with metal–semiconductor interfaces.

Acknowledgment

This work has been supported by the Fonds zur Förderung der wissenschaftlichen Forschung, Vienna, under contract no P17438-N08.

References

[1] Degond P and Mustieles F J 1991 *Solid-State Electron.* **34** 1335–45
[2] Ertler C and Schürrer F 2003 *J. Phys. A: Math. Gen.* **36** 8759–74
[3] Baranger H U and Wilkins J W 1987 *Phys. Rev.* B **36** 1487–502
[4] Fatemi E and Odeh F 1993 *J. Comput. Phys.* **108** 209–17
[5] Majorana A and Pidatella R M 2001 *J. Comput. Phys.* **174** 649–68
[6] Carrillo J A, Gamba I M, Majorana A and Shu C-W 2003 *J. Comput. Phys.* **184** 498–525
[7] Domaingo A, Galler M and Schürrer F 2005 *COMPEL—Int. J. Comput. Math. Electr. Electron. Eng.* **24** 1311–27
[8] Carrillo J A, Gamba I M, Majorana A and Shu C-W 2003 *J. Comput. Electron.* **2** 375–80
[9] Galler M and Majorana A 2005 *6th MAFPD (Kyoto) Transp. Theory Stat. Phys.* at press
[10] Sze S M 1981 *Physics of Semiconductor Devices* (New York: Wiley)
[11] Matsuzawa K, Uchida K and Nishiyama A 2000 *IEEE Trans. Electron Devices* **47** 103–8
[12] Martín M J, González T, Pardo D and Velázquez J E 1996 *Semicond. Sci. Technol.* **11** 380–7
[13] Sun L, Liu X Y, Liu M, Du G and Han R Q 2003 *Semicond. Sci. Technol.* **18** 576–81
[14] Barnham K and Vvedensky D 2001 *Low-Dimensional Semiconductor Structures: Fundamentals and Device Applications* (Cambridge: Cambridge University Press)
[15] Davies J H 1998 *The Physics of Low-Dimensional Semiconductors: An Introduction* (Cambridge: Cambridge University Press)
[16] Landau L D and Lifschitz E M 1965 *Lehrbuch der Theoretischen Physik III: Quantenmechanik* (Berlin: Akademie Verlag)
[17] Domaingo A and Schürrer F 2004 *J. Comput. Electron.* **3** 221–4
[18] Weißmantel C and Hamann C 1995 *Grundlagen der Festkörperphysik* (Heidelberg: Johann Ambrosius Barth)
[19] Sze S M 1998 *Modern Semiconductor Device Physics* (New York: Wiley)
[20] Schroeder D, Ventura D, Gnudi A and Baccarani G 1992 *Electron. Lett.* **28** 995–6
[21] Shen M, Saikin S and Cheng M-C 2004 *J. Appl. Phys.* **96** 4319–25
[22] Andrews J M and Lepselter M P 1970 *Solid-State Electron.* **13** 1011–23
[23] Shenai K and Dutton R W 1998 *IEEE Trans. Electron Devices* **35** 468–82
[24] Lapidus L and Pinter G F 1982 *Numerical Solution of Partial Differential Equations in Science and Engineering* (New York: Wiley)
[25] Jiang G-S and Shu C-W 1996 *J. Comput. Phys.* **126** 202–28
[26] Gundlach K H 1966 *Solid-State Electron.* **9** 949–57